Smart Switch Configuration and Reliability Assessment Method for Electrical Collector Systems in Offshore Wind Farms

Xiaochi Ding, *Student Member*, *IEEE*, Xinwei Shen, *Senior Member*, *IEEE*, Qiuwei Wu, *Senior Member*, *IEEE*, Liming Wang, *Senior Member*, *IEEE*, and Dechang Yang, *Member*, *IEEE*

***Abstract*—With the rapid expansion of offshore wind farms (OWFs) in remote regions, the study of highly reliable electrical collector systems (ECSs) has become increasingly important. Post-fault network recovery is considered as an effective measure of reliability enhancement. In this paper, we propose a smart switch configuration that facilitates network recovery, making it well-suited for ECSs operating in harsh environments. To accommodate the increased complexity of ECSs, a novel reliability assessment (RA) method considering detailed switch configuration is devised. This method effectively identifies the minimum outage propagation areas and incorporates post-fault network recovery strategies. The optimal normal operating state and network reconfiguration strategies that maximize ECS reliability can be obtained after optimization. Case studies on real-life OWFs validate the effectiveness and superiority of the proposed RA method compared with the traditional sequential Monte-Carlo simulation method. Moreover, numerical tests demonstrate that the proposed switch configuration, in conjunction with proper topology and network recovery, achieves the highest benefits across a wide range of operating conditions.**

***Index Terms*—Electrical collector system, mathematical programming, reliability assessment, switch configuration.**

NOMENCLATURE

A. Indices and Sets

ω	Index for wind scenarios
Ψ_N, Ψ_N^{WT}	Sets of nodes and wind turbine nodes
Ψ_C, Ψ_F	Sets of cables and feeders
Ψ_i	Set of nodes connected to node i
Ψ_I^B, Ψ_I^S	Sets of cables with breaker and switch at left end
Ψ_J^B, Ψ_J^S	Sets of cables with breaker and switch at right end
Ω	Set of wind scenarios
br^f	Index for cable connected to feeder f
f	Index for feeders
i,j,r,s,k	Indices for nodes
ij,rs	Indices for cables
TS, RS	Indices for tripped stage and recovery stage
u	Index for fault events

B. Parameters

α	Unit-price of offshore wind energy
λ_u, λ_{ij}, λ_k	Failure rates of fault u, cable ij, and wind turbine k
τ_u^{SW}, τ_u^{RP}	Time required to isolate and repair fault u
τ^{SW}, τ^{RP}	Time required to isolate and repair cable fault
τ^{WT}	Time required to repair wind turbine fault
$b_{ij}^{i,NO}$, $b_{ij}^{j,NO}$	Connection statuses of circuit breaker at nodes i and j on cable ij under normal operation
B_{ij}	Susceptance of cable ij
c_{CB}, c_{SW}	Costs of circuit breaker and isolation switch
$EENT_0$	Expected energy not transmitted of system without any breakers or switches
fr_k	Number of interruptions in power supply of wind turbine k
h_{ij}^f, h_k^f	Cable-feeder and node-feeder affiliations, 1 denoting that cable ij and wind turbine k supply power to offshore substation through feeder f
M	Big-M constant
n_{CB}, n_{SW}	Numbers of circuit breakers and isolation switches
n_f, n_n, n_c	Numbers of feeders, nodes, and cables
p^ω	Probability of scenario ω
P_f^C, P_{ij}^C	Power transmission capacities of feeder f and cable ij

Manuscript received: January 16, 2024; revised: April 5, 2024; accepted: May 28, 2024. Date of CrossCheck: May 28, 2024. Date of online publication: June 21, 2024.

This work was supported in part by National Natural Science Foundation of China (No. 52007123) and Guangdong Basic and Applied Basic Research Foundation for Offshore Wind (No. 2022A1515240019).

X. Ding and Q. Wu are with Tsinghua-Berkeley Shenzhen Institute, Tsinghua Shenzhen International Graduate School, Tsinghua University, Shenzhen, China (e-mail: dxc22@mails.tsinghua.edu.cn; qiuwu@sz.tsinghua.edu.cn).

X. Shen (corresponding author) and L. Wang are with Institute for Ocean Engineering, Tsinghua Shenzhen International Graduate School, Tsinghua University, Shenzhen, China (e-mail: xwshen@tsinghua.edu.cn; wanglm@sz.tsinghua.edu.cn).

D. Yang is with College of Information and Electrical Engineering, China Agricultural University, Beijing, China (e-mail: yangdechang@cau.edu.cn).

DOI: 10.35833/MPCE.2024.000058

P_k, R_k Sent power and rated capacity of wind turbine k

r, t Discount ratio and operating time of project

t_k^j Duration of the j^{th} interruption of wind turbine k

u_k Annual effective utilization time of wind turbines considering wake effect

C. Variables

θ_i^{rs} Voltage phase of node i when cable rs fails

$b_{ij}^{i,rs}$, $b_{ij}^{j,rs}$ Connection status of breaker at nodes i and j at tripped stage after cable rs fails

C_{rel} Reliability-related cost of offshore wind farm

$EENT$ Expected energy not transmitted

$f_{ij}^{rs,TS}$, $f_{ij}^{rs,RS}$ Virtual fault flow variables, equal to 0 when virtual fault flows through cable ij at tripped stage and reconfiguration stage after cable rs fails

$f_i^{rs,TS}$, $f_i^{rs,RS}$ Virtual fault flow variables, equal to 0 when virtual fault flows through node i at tripped stage and reconfiguration stage after cable rs fails

m_k^u, m_k^{rs} Fault impact variables, equal to 1 when wind turbine k is affected by fault u and fault of cable rs

n_k^u, n_k^{rs} Fault continuation variables, equal to 1 when wind turbine k still cannot send power after reconfiguration

P_f^{rs}, P_{ij}^{rs} Power flowing through feeder f and cable ij after reconfiguration due to fault of cable rs

P_k^{rs} Wind power sent by wind turbine k after reconfiguration following fault of cable rs

s_{ij}^{NO}, s_{ij}^{rs} Connection statuses of cable ij under normal operation and after reconfiguration following fault of cable rs

$s_{ij}^{i,rs}$, $s_{ij}^{j,rs}$ Connection statuses of isolation switch at nodes i and j at reconfiguration stage after cable rs fails

TID_k Turbine interruption duration of node k

TIF_k Turbine interruption frequency of node k

V Comprehensive benefit of switch configuration

$\widetilde{(\cdot)}$ Expected value

I. Introduction

WIND power is currently one of the fastest-growing forms of renewable energy. Offshore wind power offers several advantages over its onshore counterpart such as higher wind speeds, longer annual utilization time, and the preservation of land resources. As a result, there is potential for significant expansion of offshore wind power. The European Commission has projected that offshore wind power capacity will reach 450 GW by 2050 [1]. However, as offshore wind farms (OWFs) continue to grow in size, more cables are required to connect the wind turbines (WTs) to the power grid, increasing the vulnerability of their electrical collector systems (ECSs) [2], [3]. Submarine cables are located under the seabed, making their maintenance and repair extremely hard. Consequently, the mean time to repair (MTTR) may exceed two months [4]. Thus, high reliability of ECSs is imperative for remote and large-scale OWFs that contribute significantly to the onshore power grid, as extended fault repair time leads to considerable economic losses [5]. This highlights the necessity and importance of researching ECS reliability assessment (RA) methods [6].

The reliability analysis of power systems is well documented in the literature. Reference [7] discusses the definitions and calculation methods of reliability indices such as expected energy not supplied (EENS) and loss of load probability (LOLP). Early research on RA mainly focused on distribution networks [8] - [13]. However, with the increasing size of OWFs, RA has become indispensable for ensuring their economic and reliable operation. Currently, RA methods can be divided into time-series simulation and analytical methods. Reference [14]-[16] use Monte-Carlo simulation to evaluate the reliability of OWFs. However, applying the simulation method to the reliability of large-scale OWFs requires thousands of Monte-Carlo sample states, whose generation may greatly reduce the computational efficiency.

Various analytical methods have been studied for evaluating the reliability of OWFs [17]-[24]. One of them is based on reliability block diagram and minimal path techniques to calculate reliability indices such as EENS and annual outage hours [17], [18]. However, efficiency becomes an issue when the system is large; thus, two approximate calculation methods have been presented in [17]. Another method treats the WT string as an equivalent generator, and applies traditional reliability evaluation methods for the power grid to the availability of OWFs [19]. References [20] and [21] propose the index of generation ratio availability and its analytical calculation method to assess the performance of the ECS. Reference [22] adopts a method combining multi-state Markov process and universal generation function to assess the system reliability. Furthermore, case studies demonstrate the necessity of considering the reliability of ECS in the availability assessment of OWF. In addition, some scholars have attempted to consider reliability in wind farm planning problems [15], [16], [18], [21]. In [16], a bi-level optimization model is proposed and the sequential Monte-Carlo simulation (SMCS) is applied at the lower level to assess the reliability of the Pareto-front solutions (of wind farm layouts) obtained at the upper level. References [18] and [21] use the genetic algorithm to optimize ECS topology and calculate the reliability of optimization results analytically.

Although there have been numerous methods proposed for RA, most of them primarily focus on radial ECS with a single substation. These methods often assume traditional switch configurations [23], [24], as illustrated in Fig. 1, or completely overlook them in some cases. While [25] and [26] partially address these limitations, the detailed deployment of switches are not considered. As OWFs move towards larger-scale development, ECSs with multiple substations, complex topologies, and flexible switch configurations are becoming a trend, and the above research may not be suitable for future ECSs. It is worth noting that there are similarities between power distribution systems (PDSs) and ECSs [27]. The PDS has been studied for decades, and network recovery is verified as a powerful reliability enhance-

ment measure in PDSs [28], [29]. However, its application in ECSs has been rarely explored in the literature.

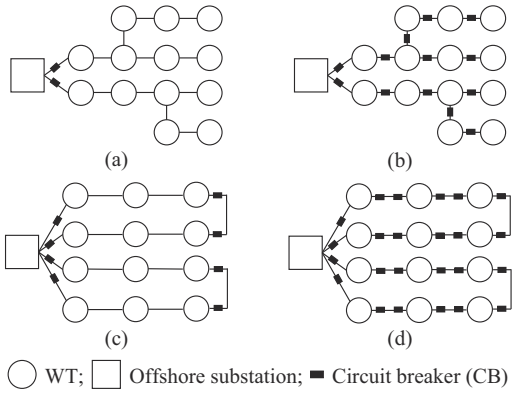

Fig. 1. Traditional switch configurations of ECS. (a) Partial switch configuration for radial ECS. (b) Complete switch configuration for radial ECS. (c) Partial switch configuration for ring ECS. (d) Complete switch configuration for ring ECS.

Additionally, most existing RA methods cannot be integrated into the planning process, as they can only be used as a posterior simulation step to check if reliability requirements are met, which inevitably leads to sub-optimal planning solutions. Therefore, an RA method compatible with ECS planning models needs to be developed to help designers balance economic efficiency and reliability.

Specifically, the comparison of the present method with existing RA methods is presented in Table I. To fill the research gap, we propose a smart switch configuration, along with an RA method for ECSs.

TABLE I
COMPARISON WITH EXISTING RA METHODS

Reference	Adaptability to complex topology	Identification of minimum outage propagation areas	Post-fault network recovery	Compatibility with planning models	Switch configuration
[15], [16]	×	×	×	√	×
[17], [18], [30]	√	×	×	√	×
[21]	√	×	×	×	√
[22]	×	√	×	×	×
[24]	×	√	×	×	√
This paper	√	√	√	√	√

The main contributions of this paper have been summarized as below.

1) A smart switch configuration suited for the ECS operating in harsh environments is devised, which supports post-fault network recovery at a relatively low cost, thereby enhancing both the economic efficiency and reliability of ECSs.

2) Correspondingly, an RA method applicable to ECS with the smart switch configuration is developed. This model offers comprehensive considerations of the identification of minimum outage propagation area and network recovery strategies, proven to be more efficient than the Monte-Carlo method. Besides performing RA of existing ECSs, it can also be integrated into the ECS planning model. The potential applicability has been demonstrated.

3) Another RA method for ECS is formulated considering detailed switch deployment based on the virtual fault flow method, and a comprehensive benefit analysis and comparison for different switch placement strategies are conducted under diverse operating conditions.

The remainder of this paper is arranged as follows. The conceptual analysis is introduced in Section II. The smart switch configuration and the associated RA method are presented in Section III. The RA method considering detailed switch deployment is formulated in Section IV. The results of case study are presented in Section V, followed by discussions in Section VI. Section VII concludes this paper.

II. CONCEPTUAL ANALYSIS

A. Calculation of Reliability Indices

To describe the system reliability, it is essential to discuss the reliability indices first. This paper utilizes the expected energy not transmitted (EENT) as a metric to characterize the overall reliability of ECS. The calculation of EENT depends on the node reliability indices, i. e., turbine interruption frequency (TIF) and turbine interruption duration (TID).

The conventional formulas for calculating TIF and TID are:

$$TIF_k = fr_k \tag{1}$$

$$TID_k = \sum_{j=1}^{fr_k} t_k^j \tag{2}$$

The above calculation method of indices requires known historical data. In the absence of historical data, RA should be conducted with a probabilistic and statistical method to obtain the expected value of reliability indices. To achieve this, we define the contingency set containing WT and cable outages, and analyze the probability and the impact of each outage. We introduce binary variables m_k^u to indicate whether the k^{th} WT is affected by the fault event u and cannot generate power, and similarly, binary variables n_k^u to indicate whether the k^{th} WT is still unable to transmit power after the network recovery from the fault event u. With these variables, we can reformulate the conventional calculations of reliability indices as:

$$TIF_k = \sum_u \lambda_u m_k^u \tag{3}$$

$$TID_k = \sum_u \lambda_u \left(\tau_u^{SW} m_k^u + \tau_u^{RP} n_k^u \right) \tag{4}$$

After obtaining the nodal reliability indices, EENT can be calculated by (5).

$$EENT = \sum_{k \in \Psi_N^{WT}} \frac{u_k R_k}{8760} \cdot TID_k \tag{5}$$

The accurate calculation of m_k^u and n_k^u is crucial for RA, necessitating a precise correlation between outage events and these variables. These aspects will be explored in depth in Sections III and IV.

B. Assumptions

The following assumptions are adopted for tractability.

1) The ECS is modeled as a graph/network, with nodes representing offshore substations or WTs, and edges representing the cable connections between them. The ECS operates radially to avoid higher fault currents in loop topology [31]. The direct current (DC) power flow model is adopted for its trade-off between computational efficiency and accuracy [30], [32].

2) The contingency set consists of cable faults and WT faults. Given the low failure rate, it is unlikely that multiple cables fail simultaneously. Hence, we assume that the cable contingency set contains only single cable outages.

3) The WTs are equipped with essential protection devices and switches capable of automatically isolating a faulty WT, thus constraining its impact on the network. Consequently, network reconfiguration is deemed unnecessary during WT faults.

III. Smart Switch Configuration and Its RA

This section presents the proposed smart switch configuration, in which the post-fault network recovery in ECS is possible, and describes how the system can reconfigure the network after a cable fault occurs. We then establish an accurate model based on mixed-integer linear programming (MILP) for ECS with the smart configuration. The model not only calculates reliability indices, but also generates optimal reconfiguration plans in fault scenarios to restore the power collection of WTs as much as possible. Therefore, it minimizes the economic loss of OWFs in fault scenarios as well (if the network reconfiguration strategies are implemented). Furthermore, this section introduces potential extended applications of the model to the ECS planning problem.

A. Post-fault Network Recovery Switch Configuration

A smart ECS switch configuration is proposed that enables network reconfiguration after faults. This configuration involves equipping each feeder with a CB at the end close to the substation, which can respond to persistent cable faults that occur anywhere in the system. Furthermore, isolation switches (SWs) are installed at both ends of all cables to isolate the local faults.

The schematic diagram of a simple ECS with the post-fault network recovery switch configuration is shown in Fig. 2(a). This system comprises one offshore substation node and five WT nodes. Solid lines represent connected cables under normal operation. WTs 2, 3, and 6 transmit power to the substation via feeder 1, while WTs 4 and 5 transmit power via feeder 2. The dotted line between WTs 3 and 5 (denoted as cable 3-5 henceforth) is the link cable, which is disconnected under normal operation. Thus, this ECS has a ring/loop topology but operates radially, consistent with Assumption 1 in Section II-B).

This system is taken as an example to demonstrate the network reconfiguration process after the cable failure. Assume that there is a persistent fault on cable 2-3. Initially, Breaker B1 on feeder 1 trips automatically, leading to WTs 2, 3, and 6 stopping transmitting power to the substation. After the duration τ^{SW}, SWs S3 and S4 on the faulty cable are disconnected to isolate the fault locally. Once the fault is isolated, B1 is reclosed, and WT 2 resumes power transmission. Next, SWs S9 and S10 on the link cable are closed, and WTs 3 and 6 resupply power to the offshore substation through feeder 2. Up to this point, the network reconfiguration is completed. After that, it takes the duration τ^{RP} for the repair crew to eliminate the fault on cable 2-3. Then, S3 and S4 are closed, S9 and S10 are opened, and the network restores the original normal operating state. The timeline is: CB tripping, fault isolation and WT resupply, and restoration to normal operation after fault clearance. Therefore, the entire process can be divided into three stages: tripped stage, (network) reconfiguration stage, and recovery stage. Figure 2(b) displays the operating statuses of WTs in all three stages.

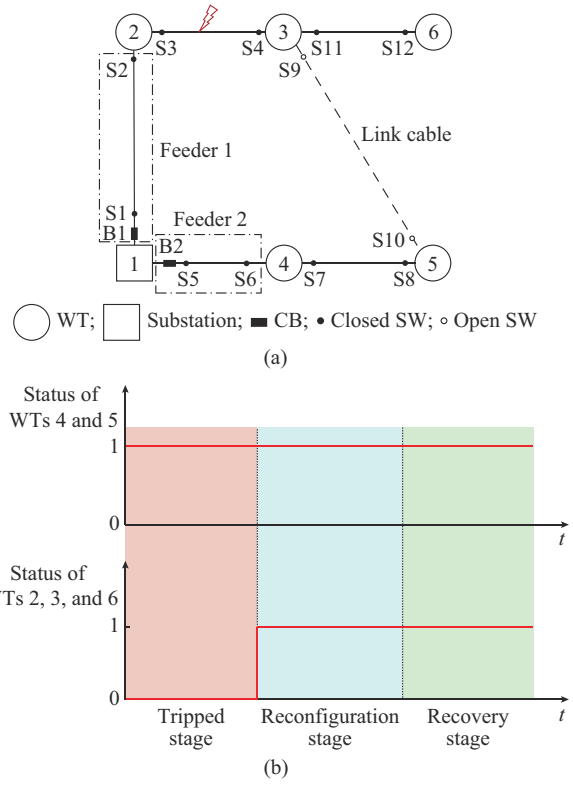

Fig. 2. Schematic diagram of a simple ECS with post-fault network recovery switch configuration. (a) Schematic diagram. (b) Statuses of WTs.

Table II summarizes the impact of all potential single cable outages in the illustrative example. It can be inferred that during a single cable fault, the WTs in the same feeder as the faulty cable are affected in the tripped stage, while other WTs are not. Most affected WTs could transmit power via another feeder after reconfiguration in the reconfiguration stage, though this is not always the case. The fifth row shows that if cable 3-6 fails, WT 6 cannot be connected to the substation through other cables, and its power transmission cannot be restored until the recovery stage.

B. The First RA Method

Considering the aforementioned network recovery process, the first RA method for the ECS with post-fault network recovery switch configuration, denoted by RA1, is formulated as (6), subject to the power flow constraints (7)-(13), outage propagation area identification constraint (14), post-fault network reconfiguration constraints (15)-(18), and reliability indices calculation constraints (19)-(22).

TABLE II
IMPACT OF ALL POTENTIAL SINGLE CABLE OUTAGES IN ILLUSTRATIVE EXAMPLE

Faulty cable	Action after failures		Duration of power supply interruption				
	Switch operation for fault isolation	Switch operation for reconfiguration	WT 2	WT 3	WT 4	WT 5	WT 6
1-2	Open B1, S1, S2	Close B1, S9, S10	τ^{SW}	τ^{SW}			τ^{SW}
2-3	Open B1, S3, S4	Close B1, S9, S10	τ^{SW}	τ^{SW}			τ^{SW}
3-6	Open B1, S11, S12	Close B1	τ^{SW}	τ^{SW}			$\tau^{SW}+\tau^{RP}$
1-4	Open B2, S5, S6	Close B2, S9, S10			τ^{SW}	τ^{SW}	
4-5	Open B2, S7, S8	Close B2, S9, S10			τ^{SW}	τ^{SW}	

$$\min_{\left\{P_{ij}^{rs},P_i^{rs},\theta_i^{rs},s_{ij}^{rs},m_k^{rs},n_k^{rs}\right\}} EENT \tag{6}$$

$$P_{ij}^{rs}=\sum_{k\in\Psi_i}\left(P_{ki}^{rs}+P_i^{rs}\right)\quad \forall i\in\Psi_N^{WT},\forall rs\in\Psi_C\cup\{NO\} \tag{7}$$

$$\left|B_{ij}\left(\theta_j^{rs}-\theta_i^{rs}\right)-P_{ij}^{rs}\right|\le\left(1-s_{ij}^{rs}\right)M\quad \forall ij\in\Psi_C,\forall rs\in\Psi_C\cup\{NO\} \tag{8}$$

$$\theta_j^{rs}=0\quad \forall j\in\Psi_N\backslash\Psi_N^{WT},\forall rs\in\Psi_C\cup\{NO\} \tag{9}$$

$$P_f^{rs}=P_{br^f}^{rs}\quad \forall f\in\Psi^F,br^f\in\Psi_C,\forall rs\in\Psi_C\cup\{NO\} \tag{10}$$

$$-Ms_{ij}^{rs}\le P_{ij}^{rs}\le Ms_{ij}^{rs}\quad \forall ij\in\Psi_C,\forall rs\in\Psi_C\cup\{NO\} \tag{11}$$

$$-P_{ij}^{C}\le P_{ij}^{rs}\le P_{ij}^{C}\quad \forall ij\in\Psi_C,\forall rs\in\Psi_C\cup\{NO\} \tag{12}$$

$$P_f^{rs}\le P_f^C\quad \forall f\in\Psi_F,\forall rs\in\Psi_C\cup\{NO\} \tag{13}$$

$$h_k^f+h_{rs}^f-1\le m_k^{rs}\quad \forall f\in\Psi_F,\forall k\in\Psi_N^{WT},\forall rs\in\Psi_C \tag{14}$$

$$s_{rs}^{rs}=0\quad \forall rs\in\Psi_C \tag{15}$$

$$m_k^{rs}\ge n_k^{rs}\quad \forall k\in\Psi_N^{WT},\forall rs\in\Psi_C \tag{16}$$

$$P_k^{rs}=P_k\left(1-n_k^{rs}\right)\quad \forall k\in\Psi_N^{WT},\forall rs\in\Psi_C \tag{17}$$

$$\sum_{ij\in\Psi_C}s_{ij}^{rs}=\sum_{k\in\Psi_N^{WT}}\left(1-n_k^{rs}\right)\quad \forall rs\in\Psi_C \tag{18}$$

$$TIF_k=\sum_{rs\in\Psi_C}\lambda_{rs}m_k^{rs}+\lambda_k\quad \forall k\in\Psi_N^{WT} \tag{19}$$

$$TID_k=\sum_{rs\in\Psi_C}\lambda_{rs}\left(\tau^{SW}m_k^{rs}+\tau^{RP}n_k^{rs}\right)+\lambda_k\tau^{WT}\quad \forall k\in\Psi_N^{WT} \tag{20}$$

$$EENT=\sum_{k\in\Psi_N^{WT}}\sum_{rs\in\Psi_C}\frac{u_kR_k}{8760}\left[\lambda_{rs}\left(\tau^{SW}m_k^{rs}+\tau^{RP}n_k^{rs}\right)+\lambda_k\tau^{WT}\right] \tag{21}$$

$$C_{rel}=\alpha\cdot EENT\cdot\frac{(1+r)^t-1}{r(1+r)^t} \tag{22}$$

It is worth noting that superscript *rs* represents different scenarios, i. e., $rs\in\Psi_C$ describes a scenario where cable *rs* (cable between WTs *r* and *s*) fails, while $rs\in\{NO\}$ represents the normal operating scenario (no fault happens).

Among them, (6)-(22) are used to describe the network reconfiguration for each cable fault scenario, thus producing $\left\{m_k^{rs}\right\}_{rs\in\Psi_C,k\in\Psi_N^{WT}}$ and $\left\{n_k^{rs}\right\}_{rs\in\Psi_C,k\in\Psi_N^{WT}}$, which can be used to calculate reliability indices as in (19)-(21). The objective function (6), with details shown in (21), aims to minimize wind power curtailment in cable and WT failure scenarios, so that the most effective fault-handling measures can be obtained accordingly.

The DC power flow model is adopted in this paper, as shown in the first block of constraints. Equation (7) is the power balance constraint. With the big-*M* method, (8) represents the phase relationship between WTs *i* and *j* when cable *ij* is connected in the fault scenario of cable *rs*. The offshore substation is set as the reference node with its voltage phase angle set to be 0, as shown in (9). Constraint (11) couples the power flow on the cable with its connection state, ensuring that the power flow is zero when the cable is disconnected. Constraints (12) and (13) limit the power flow on the cable and the feeder, respectively, below their rated capacities.

When cable *rs* fails, the CB on the feeder to which cable *rs* belongs will trip, making the WTs connected to that feeder lose power transmission capability. The outage propagation area identification constraint (14) ensures that the affected WTs cannot supply power.

Constraint (15) ensures that the faulty cable is disconnected until it is repaired. Constraint (16) means that the WTs, which have not lost power transmission capability due to CB tripping, should maintain power supply after the network is reconfigured, i. e., for any WT *k*, if $m_k^{rs}=0$, $n_k^{rs}=0$ should hold. Constraint (17) is the coupling constraint between the sent power of WTs P_k^{rs} and the fault continuation variables n_k^{rs} ($n_k^{rs}=1$ when WT *k* cannot supply power after reconfiguration), and constraint (18) ensures that the system operates radially based on its spanning tree topology.

The node reliability indices TIF and TID can be obtained by (19) and (20), respectively, while the reliability index EENT of the ECS is decided by (21). To quantify the reliability-related cost, the economic loss caused by the curtailed wind power due to cable and WT failures is calculated in (22). Therefore, with the proposed model, we could determine the optimal network recovery strategies to minimize wind power curtailment due to contingencies.

Remark: note that RA1 can be extended to incorporate the stochastic nature of WT outputs. This stochasticity can be captured using multi-scenario techniques [33]. Utilizing scenario generation and reduction methods, a comprehensive set of scenarios can be derived, denoted as $\omega\in\Omega$. Each scenario is characterized by the production levels of WTs and their respective scenario probability p^ω. Subsequently, the nodal reliability indices TIF_k^ω, TID_k^ω, and system reliability index $EENT^\omega$ for each representative scenario ω can be evaluated through the proposed model. Finally, the annualized reliability indices can be calculated by (23).

$$\begin{cases}\widetilde{TIF}_k=\sum_{\omega\in\Omega}p^\omega\cdot TIF_k^\omega\\ \widetilde{TID}_k=\sum_{\omega\in\Omega}p^\omega\cdot TID_k^\omega\\ \widetilde{EENT}=\sum_{\omega\in\Omega}p^\omega\cdot EENT^\omega\end{cases} \tag{23}$$

C. Potential Applicability of RA1

In this subsection, we will discuss how to embed RA1 into the planning model as an explicit expression of the reli-

ability of ECS whose topology could vary during the optimization process. This will assist ECS designers in achieving a balance between system economic efficiency and reliability.

Many RA methods encounter challenges when being integrated into ECS planning models due to difficulties in identifying the smallest area of outage propagation as ECS topology varies during the planning process. In RA1, this is achieved by solving for the fault impact variable of the cable m_k^{rs} ($m_k^{rs}=1$ when WT k is affected by the failure of cable rs). To address this, constraint (14) is introduced.

If the topology of ECS is known, as shown in the illustrative example in Fig. 2, both h_{rs}^f and h_k^f are parameters. And (24) can be directly obtained from the system structure diagram. Combined with (14), m_k^{rs} can be calculated as (25), which is consistent with the results in Table I.

$$\begin{cases} h_{12}^1=1, h_{12}^2=0, h_2^1=1, h_2^2=0 \\ h_{23}^1=1, h_{23}^2=0, h_3^1=1, h_3^2=0 \\ h_{36}^1=1, h_{36}^2=0, h_4^1=0, h_4^2=1 \\ h_{14}^1=0, h_{14}^2=1, h_5^1=0, h_5^2=1 \\ h_{45}^1=0, h_{45}^2=1, h_6^1=1, h_6^2=0 \end{cases} \tag{24}$$

$$\begin{cases} m_2^{12}=1, m_2^{23}=1, m_2^{36}=1, m_2^{14}=0, m_2^{45}=0 \\ m_3^{12}=1, m_3^{23}=1, m_3^{36}=1, m_3^{14}=0, m_3^{45}=0 \\ m_4^{12}=0, m_4^{23}=0, m_4^{36}=0, m_4^{14}=1, m_4^{45}=1 \\ m_5^{12}=0, m_5^{23}=0, m_5^{36}=0, m_5^{14}=1, m_5^{45}=1 \\ m_6^{12}=1, m_6^{23}=1, m_6^{36}=1, m_6^{14}=0, m_6^{45}=0 \end{cases} \tag{25}$$

If RA1 is incorporated into the OWF planning process for RA of ECSs with undetermined topology, h_{rs}^f and h_k^f become decision variables. It is necessary to describe them with the connection status variable of the cable in normal operation s_{ij}^{NO} of ECS planning. When cable ij is connected ($s_{ij}^{NO}=1$), WTs i and j, as well as cable ij, belong to the same feeder. This can be expressed as nonlinear constraint (26).

$$h_{ij}^f=s_{ij}^{NO}h_i^f=s_{ij}^{NO}h_j^f \tag{26}$$

One can linearize constraints that contain bi-linear terms to make them more manageable by applying the big-M method (the same technique is also applied to logical constraints in later sections, but will not be emphasized). By linearizing (26), we obtain (27) and (28). The source of the affiliation relationship is given by (29). And if cable ij is disconnected under normal operation ($s_{ij}^{NO}=0$), it is called link cable. Link cables do not belong to any feeder, as indicated in (30).

$$\left|h_{ij}^f-h_i^f\right|\le M\left(1-s_{ij}^{NO}\right) \quad \forall ij\in\Psi_C, \forall f\in\Psi_F \tag{27}$$

$$\left|h_{ij}^f-h_j^f\right|\le M\left(1-s_{ij}^{NO}\right) \quad \forall ij\in\Psi_C, \forall f\in\Psi_F \tag{28}$$

$$h_{br^f}^f=s_{br^f}^{NO} \quad \forall f\in\Psi_F, br^f\in\Psi_C \tag{29}$$

$$h_{ij}^f\le s_{ij}^{NO} \quad \forall f\in\Psi_F, \forall ij\in\Psi_C \tag{30}$$

$$0\le h_k^f\le 1 \quad \forall k\in\Psi_N^{WT}, \forall f\in\Psi^F \tag{31}$$

$$0\le h_{ij}^f\le 1 \quad \forall ij\in\Psi_C, \forall f\in\Psi^F \tag{32}$$

$$\sum_f h_k^f\le 1 \quad \forall k\in\Psi_N^{WT} \tag{33}$$

$$\sum_f h_{ij}^f\le 1 \quad \forall ij\in\Psi_C \tag{34}$$

Thus, the potential application of RA1 in the field of ECS network planning and operation can be achieved with the constraints above. Since the model is an MILP problem, its computational efficiency is determined by the number of binary variables. To reduce this, we set h_{ij}^f and h_k^f as continuous variables during the modeling, and introduce coupling constraints with binary variables using (27)-(30). Their value ranges are specified by (31)-(34), limiting h_{ij}^f and h_k^f to binary values of 0 or 1. The total number of binary variables in the RA1 is reduced by $n_f n_n+n_f n_c$, thereby improving the computational efficiency of the RA1.

IV. RA of ECS Considering Detailed Switch Deployment

To investigate the impact of switch configuration on the reliability of ECS, i. e., the deployment of CBs and SWs, and to assess whether the proposed smart switch configuration is a worthwhile investment, we extend the RA1 to consider the flexible placement of switch devices using the virtual fault flow (VFF) method.

A. Description of VFF Method

VFF refers to the simulated propagation of "fault flow" in cable fault scenarios, which enables evaluation of outage ranges. Essentially, VFF simulates the isolation of the fault area by switch devices in the ECS, causing the part that the VFF flows through to experience a blackout. VFF arises from the faulty cable and is classified into two types based on the stage of the fault: ① tripped stage virtual fault flow (TSVFF); and ② reconfiguration stage virtual fault flow (RSVFF). TSVFF can be interrupted by open SWs during normal operation and tripped CBs, while RSVFF can be interrupted by open SWs during the reconfiguration stage, as illustrated in Fig. 3.

When cable 2-3 in Fig. 3 experiences a persistent fault and breaker B1 automatically trips, the system enters into the tripped stage. TSVFF originates from cable 2-3 and spreads to both sides. TSVFF is blocked by the tripped B1 when it spreads upstream. As S11 and S12 are closed, while S9 and S10 are open during normal operation, TSVFF can propagate downstream along cable 3-6 only. Once the switches are operated by the OWF operator, the ECS enters into the reconfiguration stage. RSVFF arises from cable 2-3 and is restricted between S3 and S4 since the two SWs are open at this stage.

B. The Second RA Method

The second RA method (denoted by RA2), which considers flexible switch deployment, also includes TIF, TID, and EENT as reliability indices. The objective function is consistent with (6) and (21), aimed at obtaining reconfiguration strategies that result in the least wind power curtailment in various fault scenarios. RA2 is formulated as follows.

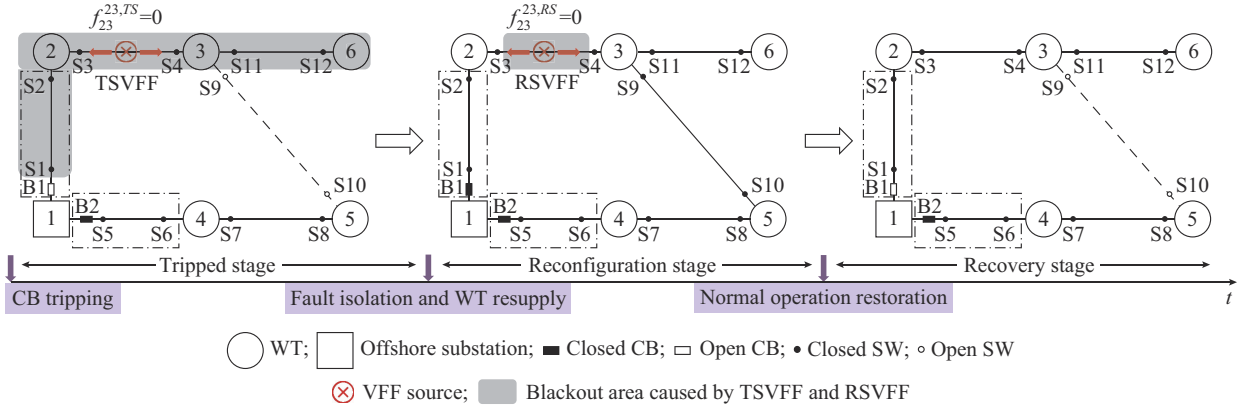

Fig. 3. Framework of VFF.

$$\min_{\substack{\{P_{ij}^{rs},P_i^{rs},\theta_i^{rs},b_{ij}^{i,rs},b_{ij}^{j,rs},s_{ij}^{i,rs},s_{ij}^{j,rs},s_{ij}^{rs},\\ f_{ij}^{rs,TS},f_{ij}^{rs,RS},f_i^{rs,TS},f_i^{rs,RS},m_k^{rs},n_k^{rs}\}}} EENT \tag{35}$$

The constraints can be divided into four parts. The first two parts simulate the VFF propagation in different stages. To be more specific, the first part of constraints is about the spread of TSVFF in the tripped stage:

$$f_{rs}^{rs,TS}=0 \quad \forall rs\in\Psi_C \tag{36}$$

$$\left|f_{ij}^{rs,TS}-f_i^{rs,TS}\right|\le\left(1-b_{ij}^{i,rs}\right)M \quad \forall ij\in\Psi_I^B,\forall rs\in\Psi_C \tag{37}$$

$$\left|f_{ij}^{rs,TS}-f_i^{rs,TS}\right|\le\left(1-s_{ij}^{i,NO}\right)M \quad \forall ij\in\Psi_I^S,ij\notin\Psi_I^B,\forall rs\in\Psi_C \tag{38}$$

$$f_{ij}^{rs,TS}=f_i^{rs,TS} \quad \forall ij\notin\Psi_I^S,ij\notin\Psi_I^B,\forall rs\in\Psi_C \tag{39}$$

$$\left|f_{ij}^{rs,TS}-f_j^{rs,TS}\right|\le\left(1-b_{ij}^{j,rs}\right)M \quad \forall ij\in\Psi_J^B,\forall rs\in\Psi_C \tag{40}$$

$$\left|f_{ij}^{rs,TS}-f_j^{rs,TS}\right|\le\left(1-s_{ij}^{j,NO}\right)M \quad \forall ij\in\Psi_J^S,ij\notin\Psi_J^B,\forall rs\in\Psi_C \tag{41}$$

$$f_{ij}^{rs,TS}=f_j^{rs,TS} \quad \forall ij\notin\Psi_J^S,ij\notin\Psi_J^B,\forall rs\in\Psi_C \tag{42}$$

$$0\le f_i^{rs,TS}\le 1 \quad \forall i\in\Psi_N^{WT},\forall rs\in\Psi_C \tag{43}$$

$$0\le f_{ij}^{rs,TS}\le 1 \quad \forall ij\in\Psi_C,\forall rs\in\Psi_C \tag{44}$$

$$f_i^{rs,TS}=1 \quad \forall i\in\Psi_N\backslash\Psi_N^{WT},\forall rs\in\Psi_C \tag{45}$$

$$\sum_{ij\in\Psi_I^B}\left|b_{ij}^{i,NO}-b_{ij}^{i,rs}\right|+\sum_{ij\in\Psi_J^B}\left|b_{ij}^{j,NO}-b_{ij}^{j,rs}\right|\le 1 \quad \forall rs\in\Psi_C \tag{46}$$

$$m_k^{rs}=1-f_k^{rs,TS} \quad \forall k\in\Psi_N^{WT},\forall rs\in\Psi_C \tag{47}$$

As mentioned earlier, TSVFF arises from the faulty cable, which is described in (36). Its propagation in ECS is impacted by CBs and SWs. Only the CBs that trip during the TS or the SWs that are disconnected in normal operating condition can interrupt the spread of TSVFF, and constraints (37)-(42) describe this using big-*M* method. To reduce the number of binary variables, the same method as in Section III-C is adopted. The VFF variables are defined as continuous variables, and their values are limited by constraints (44) and (45). Constraint (46) emphasizes that there should be at most one CB trip action after cable fault occurs. Constraint (47) denotes the relationship between the fault impact variables and the TSVFF variables.

The second part of constraints is about the spread of RSVFF in the reconfiguration stage:

$$f_{rs}^{rs,RS}=0 \quad \forall rs\in\Psi_C \tag{48}$$

$$\left|f_{ij}^{rs,RS}-f_i^{rs,RS}\right|\le\left(1-s_{ij}^{i,rs}\right)M \quad \forall ij\in\Psi_I^S,\forall rs\in\Psi_C \tag{49}$$

$$f_{ij}^{rs,RS}=f_i^{rs,RS} \quad \forall ij\notin\Psi_I^S,\forall rs\in\Psi_C \tag{50}$$

$$\left|f_{ij}^{rs,RS}-f_j^{rs,RS}\right|\le\left(1-s_{ij}^{j,rs}\right)M \quad \forall ij\in\Psi_J^S,\forall rs\in\Psi_C \tag{51}$$

$$f_{ij}^{rs,RS}=f_j^{rs,RS} \quad \forall ij\notin\Psi_J^S,\forall rs\in\Psi_C \tag{52}$$

$$0\le f_i^{rs,RS}\le 1 \quad \forall i\in\Psi^{WT},\forall rs\in\Psi_C \tag{53}$$

$$0\le f_{ij}^{rs,RS}\le 1 \quad \forall ij\in\Psi_C,\forall rs\in\Psi_C \tag{54}$$

$$f_i^{rs,RS}=1 \quad \forall i\in\Psi_N\backslash\Psi_N^{WT},\forall rs\in\Psi_C \tag{55}$$

$$n_k^{rs}=1-f_k^{rs,RS} \quad \forall k\in\Psi_N^{WT},\forall rs\in\Psi_C \tag{56}$$

Similarly, RSVFF arises from the faulty cable, as described in (48). Its propagation within the ECS is impacted by SWs. Only the SWs that are disconnected during the RS could interrupt the spread of RSVFF. This is described by constraints (49)-(52). RSVFF variables are defined as continuous variables with their values restricted by constraints (53)-(55). Constraint (56) denotes the relationship between the fault continuation variables and RSVFF variables.

The operating constraints in fault scenarios are formulated in the third part, which are similar to RA1.

$$\begin{cases}(7)\text{-}(13) & \forall rs\in\Psi_C\cup\{NO\}\\ (16)\text{-}(18) & \forall rs\in\Psi_C\end{cases} \tag{57}$$

$$s_{ij}^{rs}=1 \quad \forall ij\notin\Psi_I^S,ij\notin\Psi_J^S \tag{58}$$

$$s_{ij}^{rs}=s_{ij}^{i,rs} \quad \forall ij\in\Psi_I^S,ij\notin\Psi_J^S \tag{59}$$

$$s_{ij}^{rs}=s_{ij}^{j,rs} \quad \forall ij\in\Psi_J^S,ij\notin\Psi_I^S \tag{60}$$

$$\begin{cases}s_{ij}^{rs}\le s_{ij}^{i,rs}\\ s_{ij}^{rs}\le s_{ij}^{j,rs}\\ s_{ij}^{rs}\ge s_{ij}^{i,rs}+s_{ij}^{j,rs}-1\end{cases} \quad \forall ij\in\Psi_I^S,ij\in\Psi_J^S \tag{61}$$

But due to the consideration of detailed switch deployment, the connectivity status of the cable depends on the connectivity status of its corresponding switches, as described in (58)-(61).

The fourth part of constraints calculates the reliability indices and comprehensive benefits of switch configurations:

$$\begin{cases} (19)\text{-}(22) \\ V = \dfrac{\alpha(1+r)^t - 1}{r(1+r)^t}\left(EENT_0 - EENT\right) - \left(c_{CB}n_{CB} + c_{SW}n_{SW}\right) \end{cases} \quad (62)$$

The overall benefit of switch configuration, denoted by V in (62), is defined as the benefit of reliability improvement $\alpha\left(EENT_0 - EENT\right)\dfrac{(1+r)^t - 1}{r(1+r)^t}$ minus the cost of purchasing and installing all switch devices $c_{CB}n_{CB} + c_{SW}n_{SW}$. Obviously, the benefit brought by reliability improvement is equal to the difference between the blackout costs of the no-switch configuration $EENT_0$ and the current configuration $EENT$. The present value of the overall benefit is considered by multiplying a coefficient $\dfrac{(1+r)^t - 1}{r(1+r)^t}$.

Note that, both RA1 and RA2 are formulated and transformed into MILP forms, which can be easily solved by modern branch-and-cut solvers.

V. Case Study

The proposed RA1 and RA2 are applied and verified in this section. Firstly, we study the influence of post-fault network reconfiguration as well as the system operating state on the reliability at the Ormonde OWF. Next, we apply RA1 to examine the impact of ECS topology on reliability at the Hornsea One Centre OWF. Then, we assess the reliability of the Beatrice OWF equipped with six different switch configurations with RA2. Finally, the scalability of the proposed method is validated at the London Array OWF. The information on real OWFs and wind resources are obtained from [34] and [35], respectively. A two-dimensional Jensen model with a Gaussian-shaped velocity deficit is utilized to characterize the wake effect. More details on this model can be found in [36]. For ease of reproducibility, the detailed data including information on WTs and cables are available in [37]. Simulations are implemented on a laptop PC with an Intel Core i5 processor using Gurobi 10.0.0. The optimality tolerance is set to be 0 so that all cases are solved to optimality.

A. Effect of Post-fault Network Reconfiguration on Reliability

In order to study the effect of post-fault network reconfiguration on reliability, we perform RA on Ormonde OWF shown in Fig. 4. Two RA methods, i.e., RA method without considering network reconfiguration (M1) and RA1, are utilized for comparison.

We adopt two methods to obtain various operating states for the radial and ring ECSs, respectively. One method involves sequentially removing two cables in Fig. 4 to form the radial topology and treating it as the normal operating state of the radial ECSs. The other method obtains the operating states conforming to the assumption of radial operation by sequentially selecting two specific cables in Fig. 4 as the normally disconnected cables (link cables). Then M1 and RA1 are applied to each operating state, and Table III shows the comparison of the system reliability index with and without considering post-fault network reconfiguration.

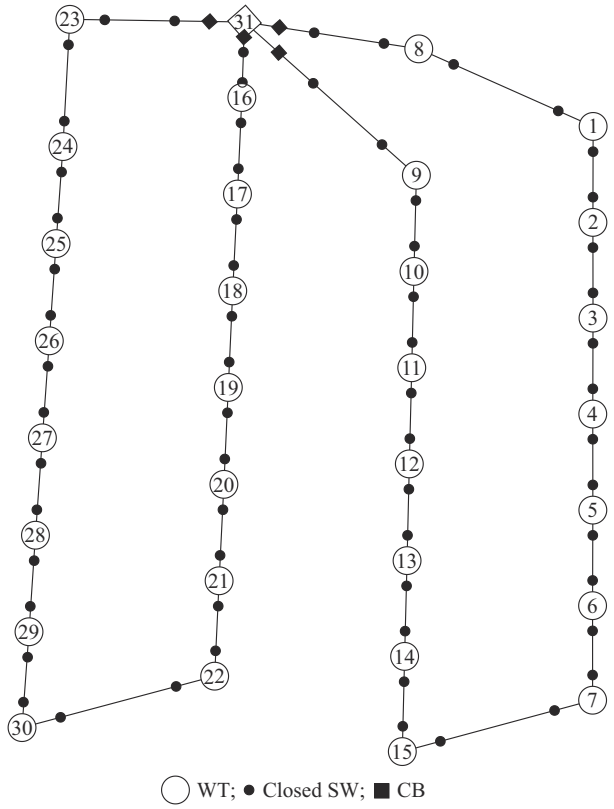

Fig. 4. ECS of Ormonde OWF.

TABLE III
Influence of Network Reconfiguration on Reliability

Radial ECS (M1 without considering network reconfiguration)		Ring ECS (RA1 considering network reconfiguration)	
Removed cable *i-j*	*EENT* (MWh/year)	Link cable *i-j*	*EENT* (MWh/year)
9-10, 16-17	8965.50	9-10, 16-17	99.98
10-11, 17-18	8072.66	10-11, 17-18	93.57
11-12, 18-19	7337.76	11-12, 18-19	88.17
12-13, 19-20	6734.84	12-13, 19-20	83.69
13-14, 20-21	6231.46	13-14, 20-21	80.04
14-15, 21-22	5867.81	14-15, 21-22	77.37
7-15, 22-30	5623.95	7-15, 22-30	74.33
6-7, 29-30	5632.07	6-7, 29-30	75.05
5-6, 28-29	5809.69	5-6, 28-29	75.97
4-5, 27-28	6140.69	4-5, 27-28	77.98
3-4, 26-27	6619.79	3-4, 26-27	81.06
2-3, 25-26	7284.63	2-3, 25-26	85.33
1-2, 24-25	8114.11	1-2, 24-25	90.74
1-8, 23-24	9235.89	1-8, 23-24	97.69

It is evident from Table III that the ECS exhibits varying reliability levels depending on its normal operating states. And the proposed method offers a way to identify the most reliable operating state. The reliability index comparison demonstrates that the ring ECS and the implementation of network reconfiguration lead to a much more reliable OWF.

By comparing the reliability results for each type of ECS, it can be observed that the highest reliability is achieved when cables 7-15 and 22-30 are chosen as the "removed cables" or "link cables", while the lowest reliability is achieved when cables 9-10 and 16-17 are selected as the "removed cables" or "link cables". Based on Table III and Fig. 4, it can be concluded that when WTs are more evenly distributed on different feeders under normal operation, it is more likely to achieve a lower reliability index EENT, namely, a more reliable ECS.

The impact of the stochasticity of WTs on the ECS reliability is also investigated. The most reliable operating states (with the lowest *EENT*) in Table III are taken for illustration. Given that the MTTR is relatively long, the short-term fluctuations in WT output should have a minimal impact on reliability. Hence, we have extracted six representative scenarios from the monthly wind profile [35] to characterize the long-term variability of wind, as shown in Fig. 5. Scenario probabilities and corresponding ECS reliability indices obtained through RA method are listed in Table IV. By employing (23), the indices $\widehat{EENT}$ for radial and ring ECSs are 5615.30 MWh/year and 74.21 MWh/year, respectively. A comparison with Table III reveals a slight deviation due to WT output stochasticity, indicating its minor effect on the RA process. Therefore, to simplify and maintain focus on pivotal aspects, WT output uncertainty will not be explicitly modeled in subsequent simulation.

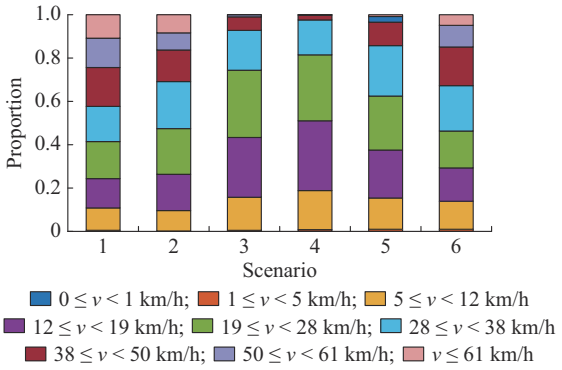

Fig. 5. Stochastic scenarios of wind speed.

TABLE IV
INFLUENCE OF STOCHASTICITY OF WT OUTPUT ON RELIABILITY

Scenario	p^{ω} (%)	$EENT^{\omega}$ for radial ECS (MWh/year)	$EENT^{\omega}$ for ring ECS (MWh/year)
1	16.164	7075.57	93.52
2	16.712	6473.45	85.56
3	16.712	4586.10	60.61
4	16.988	4144.30	54.77
5	16.712	5140.63	67.94
6	16.712	6343.93	83.85

B. Effect of Topology on Reliability

In this subsection, the impact of the ECS topology on reliability indices is investigated by adding link cables to the system. To maintain experimental consistency, the reliability of various topologies is assessed under the most reliable operating states as determined from the findings in Section V-A. The study is conducted on the Hornsea One Centre OWF, whose structure is given in Supplementary Material A. It comprises nine link cables identified as R1-R9. Ten interrelated yet distinct cases are designed as described below. Case 1 represents a radial ECS without any link cables. From Cases 2-10, one link cable is added to the previous case in the order of R1-R9. As such, Case 10 contains all nine link cables.

To validate the feasibility of RA1, we compare it with the SMCS method introduced in [16]. Table V summarizes the results of ten cases based on the RA1 and SMCS methods, respectively. It can be observed that the reliability indices of the two methods are basically consistent. But RA1 outperforms the SMCS method in terms of solution speed, with an average computation time of 1.3 s, compared with 14.9 s for the SMCS method.

TABLE V
RESULTS OF TEN CASES BASED ON *RA*1 AND SMCS METHODS

Case	*EENT* of RA1 (MWh/year)	*EENT* of SMCS (MWh/year)	Computation time of RA1 (s)	Computation time of SMCS (s)
1	55761	55795	1.13	13.50
2	45736	45813	0.78	13.18
3	40153	40220	1.00	14.52
4	33143	33177	0.92	14.38
5	26323	26350	1.17	14.09
6	20795	20825	0.98	17.57
7	13902	13947	1.71	16.23
8	3568	3577	2.14	16.90
9	2805	2810	1.13	13.01
10	2805	2807	1.95	15.53

Compared with the SMCS method that requires thousands of samples, RA1 significantly accelerates the computation speed. To gain a more comprehensive view of RA1, it is compared with other commonly utilized analytical RA methods.

A power flow based RA method for ECSs, labeled as M2, has been widely adopted in [4], [38] - [40]. As detailed in [38], M2 calculates the reliability indices by considering the power flowing through each cable, along with their respective failure rates and repair times. Additionally, another non-simulation-based RA method in [9] has been modified to assess the reliability of ECS, accounting for the failures of both cables and WTs. This method is denoted as M3. Upon applying M2 to assess the reliability of Cases 1-10, the results are uniformly 55986 MWh/year, while M3 consistently yields results of 55761 MWh/year. In the case of the radial ECS (Case 1), the EENTs obtained by M2 and M3 closely match or equal to that determined by RA1. However, neither M2 nor M3 takes into account strategies for post-fault network reconfiguration, which results in unchanged results across Cases 2-10. This observation indicates that both M2

and M3 significantly underestimate the reliability of ECSs incorporating link cables. Additionally, [30] asserts that ECSs with a double-sided ring topology incur no wind power curtailment in the event of cable faults, implying an assumption of instantaneous fault detection and isolation. However, this assumption does not entirely coincide with practical scenarios, thereby resulting in an overestimated assessment of the system reliability.

In contrast to the aforementioned methods, RA1 comprehensively considers the procedures for fault detection, isolation, and network reconfiguration. This facilitates a more precise assessment of the reliability of ECSs. Moreover, RA1 is versatile and can be adapted to address a wider range of fault scenarios, which will be discussed in Section VI. It is clear that the topology has a significant impact on system reliability. Case 10 has an EENT of 2805 MWh, which is only 5.0% of Case 1. This effectiveness arises because, although link cables are not active during normal operations, they facilitate network reconfiguration following sustained faults, thereby enabling some fault-affected WTs to resupply power during the reconfiguration stage. The benefit is reflected by the nodal reliability indices of Cases 1 and 10 in Fig. 6.

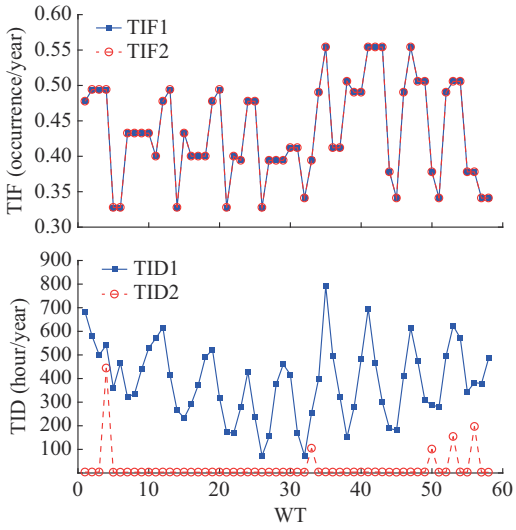

Fig. 6. Nodal reliability indices comparison of Cases 1 and 10.

Figure 6 compares the reliability metrics of WTs in Case 1 (TIF1 and TID1) and Case 10 (TIF2 and TID2). In Case 1, if cable 38-59 fails, the five WTs (38, 48, 49, 53, 54) connected to this cable cannot transmit power until the fault is fully cleared. By contrast, in Case 10, the power generated by these WTs could be transmitted to the substation via the link cable R6 within its capacity limits, thus greatly increasing the ability of ECS to reduce wind power curtailment. As shown in Fig. 6, investing in link cables has no impact on TIF. And the main benefit is to reduce TID by supporting reconfiguration after cable faults.

The power flow distribution in fault scenarios of Case 10 is presented in Fig. 7. It shows that power flows on the cables are bidirectional and adhere to security operating restrictions.

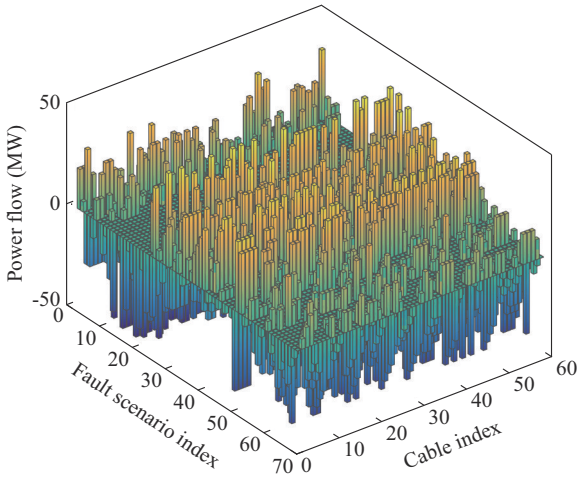

Fig. 7. Power flow under various fault scenarios of Case 10.

It should be stressed that while generally laying more link cables in the ECS significantly improves reliability, there are also cases where it does not. This diminishing marginal utility is reflected in the last three rows of Table V. Laying R8 slightly improves the reliability, reducing EENT by only 763 MWh. Moreover, installing R9 makes no difference to the reliability. When the current link cables suffice for network reconfiguration, laying R9 only elevates investment without altering optimal strategies, making it an unsuitable investment. The cost of laying marine cables can be expensive in actual projects. Therefore, when planning an ECS that does not require high reliability, it is necessary to strike a balance between economic efficiency and reliability.

C. Effect of Switch Configuration on Reliability

This subsection aims to verify RA2 considering flexible switch configurations proposed in Section IV. The RA2 is highly flexible and can be applied to ECS with multiple substations. To evaluate the impact of switch configuration, we assess the reliability indices and comprehensive benefits for six cases on Beatrice OWF, as illustrated in Table VI and Supplementary Material A.

TABLE VI
DETAILS OF CASES WITH DIFFERENT SWITCH CONFIGURATIONS

Case	Link cable	Deployment of CBs	Deployment of SWs
1	√	Upstream of feeders	Both ends of all cables
2		Upstream of feeders	Both ends of all cables
3	√	Upstream of feeders and upstream of selected cables	Both ends of all cables
4	√	Upstream of feeders and downstream of selected cables	Both ends of all cables
5	√	Upstream of feeders	Upstream of all cables and both ends of link cables
6	√	Upstream of feeders	Upstream of feeders and both ends of link cables

The results are presented in Table VII. Additionally, $EENT_0$ (as shown in (61)) of the base case without any switch device, is also calculated. If VFF propagation is not

blocked by any switch device, any fault would lead to a system-wide power outage. This causes a significant curtailment, amounting to 887082 MWh or 40% of the annual power generation.

TABLE VII
COMPARISON OF RELIABILITY INDICES AND COMPREHENSIVE BENEFITS

Case	*EENT* (MWh)	*V* (k$)	Computation time (s)
1	289.34	886053	3.10
2	37955.62	848430	2.20
3	235.32	885862	3.18
4	252.37	885845	2.91
5	10830.73	875772	1.91
6	63516.91	823323	1.30

The results lead to several key conclusions as follows.

1) Comparing the base case and Cases 1-6, installing switches in ECS greatly improves the system reliability, resulting in significant benefits. Even only installing CBs and SWs on feeders (as in Case 6) greatly reduces power curtailment.

2) With the same switch configuration, link cables facilitate system reconfiguration, as shown by the comparison between Cases 1 and 2, leading to further power curtailment reductions.

3) Comparing Cases 1 and 3/4, installing sectional CBs reduces the TSVFF propagation range and the number of affected WTs in TS, improving the system reliability. And placing sectional CBs upstream provides greater benefits. But the installation of sectional CBs is a bit less economical due to the high cost.

4) Comparing Cases 1 and 5/6, deploying SWs at both ends of cables facilitates the rapid isolation of faulty areas and reduces the propagation range of RSVFF. The bilateral configuration of SWs increases the number of WTs that can recover power supply in RS and improves system reliability.

Clearly, the strategic deployment of switch devices profoundly influences the reliability of ECSs. Case 3 is the most reliable, while Case 1 has the highest comprehensive benefit.

The failure rate (FR) and MTTR are important parameters that impact system reliability. To comprehensively consider their fluctuations in different operational environments, the sensitivity analysis of cable FR and MTTR has been conducted. The results are presented in Fig. 8.

The color bar corresponds to different switch configurations. As a moderate investment option, the proposed switch configuration provides a balanced method. It consistently yields the highest benefits under a wide range of conditions. In nearshore areas with favorable operating conditions and relatively short fault repair time, a unilateral deployment of SWs is sufficient. However, in extremely harsh environments where both FR and MTTR are quite high, it is necessary to invest in bilateral SWs and even sectional CBs to reduce power curtailment and achieve greater benefits.

The sensitivity analysis offers investment insights for OWF operators and highlights the potential value of implementing the proposed switch configuration. Therefore, it could be a worthwhile investment to consider.

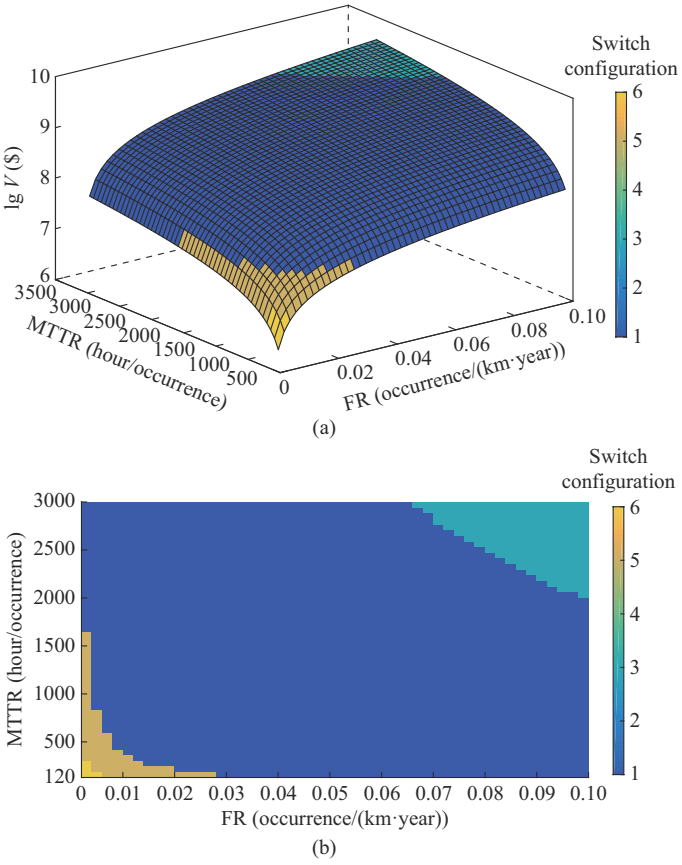

Fig. 8. Sensitivity analysis of FR and MTTR. (a) Three-dimensional view. (b) Top view.

D. Scalability Validation of Models

To validate the scalability of RA1 and RA2, we extend the analysis to the London Array OWF, one of the world's largest OWFs, featuring two substations and 175 WTs. The ECS layout for this OWF is illustrated in Supplementary Material A. Under the assumption of implementing the proposed switch configuration, both methods can perform the RA.

Both RA1 and RA2 yield an EENT of 566.494 MWh/year. However, RA1 is faster with a solution time of 9.33 s, while RA2 takes 12.03 s. This indicates that RA1 is more suitable for ECS with the proposed switch configuration. Additionally, both models have proven effective in assessing the reliability of large ECS, showing their scalability for broad applications.

VI. DISCUSSIONS

The repeated tests show that both proposed RA methods can obtain the optimal solution quickly within a few seconds. The RA1 is easier to solve and is suitable for assessment of the proposed switch configuration. The RA2 considers more details, resulting in more variables and constraints. It is recommended for analyzing the reliability of other configurations.

Furthermore, RA1 and RA2 demonstrate good scalability and adaptability to various equipment faults. Detailed discussions on these aspects can be found in Supplementary Material A.

VII. Conclusion

This paper introduces a smart switch configuration that enables network reconfiguration at a reduced cost. This configuration is particularly effective for ECSs requiring high reliability. In conjunction, we present an RA method that demonstrates superior performance compared with the SMCS method. Furthermore, to evaluate various switch deployment strategies, another RA method is developed that accounts for the detailed placement of CBs and SWs. Numerical tests reveal that the smart switch configuration achieves the highest benefits under a wide range of operating conditions.

The conclusions from numerical tests are threefold.

1) Investing in link cables generally enhances ECS reliability, although the benefits diminish as the number of link cables increases beyond a certain threshold.

2) Once the ECS topology is determined, the system reliability depends on the switch configuration and normal operating state, i. e., how switch devices are placed and how evenly WTs are distributed under normal operation. The application of post-fault reconfiguration strategies contributes largely to enhancing the system reliability.

3) It is worth noting that by linearization, both RA methods are transformed into MILP, which can be easily solved by branch-and-cut solvers within seconds.

This paper assesses the reliability of multiple ECSs, with a current focus on permanent faults and steady-state operations. Acknowledging these limitations, future research will aim to incorporate the effects of transient faults to furnish a more comprehensive understanding of system reliability. Another limitation of the proposed RA method, similar to the majority of the literature, lies in the assumption of constant failure rates and repair times for equipment. In practice, however, both parameters may vary over time. Only [18] has discussed the estimation formula, yet it still relies on time-constant parameters to enhance computational efficiency. This represents a common shortfall in current research and will be addressed in our future studies for improvement.

Considering the potential integration of RA methods with planning frameworks, future research should focus on planning models that concurrently optimize cable layouts, switch configurations, and overall system reliability. This could significantly enhance the economic efficiency and reliability of ECSs.

References

[1] K. Freeman, C. Frost, G. Hundleby *et al.* (2019, Nov.). Our energy our future − how offshore wind will help Europe go carbon-neutral. [Online]. Available: https://windeurope. org/intelligence-platform/product/our-energy-our-future/

[2] C. Berzan, K. Veeramachaneni, J. McDermott *et al.*, "Algorithms for cable network design on large-scale wind farms," Tech. Rep., Massachusetts Institute of Technology, Cambridge, USA, 2011.

[3] H. Badihi, Y. Zhang, and H. Hong, "Fault-tolerant cooperative control in an offshore wind farm using model-free and model-based fault detection and diagnosis approaches," *Applied Energy*, vol. 201, pp. 284-307, Sept. 2017.

[4] T. Zuo, "Optimal planning for wind farm collector system," Ph.D. dissertation, School of Electrical Engineering and Telecommunications, University of New South Wales, Sydney, Australia, 2020.

[5] B. Zhang and Z. Zhang, "A two-stage model for asynchronously scheduling offshore wind farm maintenance tasks and power productions," *International Journal of Electrical Power & Energy Systems*, vol. 130, p. 107013, Sept. 2021.

[6] P. Hou, J. Zhu, K. Ma *et al.*, "A review of offshore wind farm layout optimization and electrical system design methods," *Journal of Modern Power Systems and Clean Energy*, vol. 7, no. 5, pp. 975-986, Sept. 2019.

[7] R. N. Allan, *Reliability Evaluation of Power Systems*. New York: Springer Science & Business Media, 2013, pp. 68-73.

[8] G. T. Heydt and T. J. Graf, "Distribution system reliability evaluation using enhanced samples in a Monte Carlo approach," *IEEE Transactions on Power Systems*, vol. 25, no. 4, pp. 2006-2008, Nov. 2010.

[9] G. Muñoz-Delgado, J. Contreras, and J. M. Arroyo, "Reliability assessment for distribution optimization models: a non-simulation-based linear programming approach," *IEEE Transactions on Smart Grid*, vol. 9, no. 4, pp. 3048-3059, Nov. 2016.

[10] J. C. López, M. Lavorato, and M. J. Rider, "Optimal reconfiguration of electrical distribution systems considering reliability indices improvement," *International Journal of Electrical Power & Energy Systems*, vol. 78, pp. 837-845, Jun. 2016.

[11] G. M. Delgado, J. Contreras, and J. M. Arroyo, "Distribution network expansion planning with an explicit formulation for reliability assessment," *IEEE Transactions on Power Systems*, vol. 33, no. 3, pp. 2583-2596, Oct. 2017.

[12] Z. Li, W. Wu, and B. Zhang, "Analytical reliability assessment method for complex distribution networks considering post-fault network reconfiguration," *IEEE Transactions on Power Systems*, vol. 35, no. 2, pp. 1457-1467, Aug. 2019.

[13] Z. Li, W. Wu, X. Tai *et al.*, "A reliability-constrained expansion planning model for mesh distribution networks," *IEEE Transactions on Power Systems*, vol. 36, no. 2, pp. 948-960, Aug. 2020.

[14] X. Han, Y. Qu, P. Wang *et al.*, "Four-dimensional wind speed model for adequacy assessment of power systems with wind farms," *IEEE Transactions on Power Systems*, vol. 28, no. 3, pp. 2978-2985, Dec. 2012.

[15] Y.-K. Wu, P.-E. Su, Y.-S. Su *et al.*, "Economics-and reliability-based design for an offshore wind farm," *IEEE Transactions on Industry Applications*, vol. 53, no. 6, pp. 5139-5149, Aug. 2017.

[16] S. Paul and Z. H. Rather, "A new bi-level planning approach to find economic and reliable layout for large-scale wind farm," *IEEE Systems Journal*, vol. 13, no. 3, pp. 3080-3090, Feb. 2019.

[17] O. Dahmani, S. Bourguet, M. Machmoum *et al.*, "Reliability analysis of the collection system of an offshore wind farm," in *Proceedings of 2014 Ninth International Conference on Ecological Vehicles and Renewable Energies (EVER)*, Monte-Carlo, Monaco, Mar. 2014, pp. 1-6.

[18] O. Dahmani, S. Bourguet, M. Machmoum *et al.*, "Optimization and reliability evaluation of an offshore wind farm architecture," *IEEE Transactions on Sustainable Energy*, vol. 8, no. 2, pp. 542-550, Sept. 2017.

[19] L. Huang and Y. Fu, "Reliability evaluation of the offshore wind farm," in *Proceedings of 2010 Asia-Pacific Power and Energy Engineering Conference*, Chengdu, China, Mar. 2010, pp. 1-5.

[20] M. Zhao, Z. Chen, and F. Blaabjerg, "Generation ratio availability assessment of electrical systems for offshore wind farms," *IEEE Transactions on Energy Conversion*, vol. 22, pp. 755-763, Sept. 2007.

[21] M. Zhao, Z. Chen, and F. Blaabjerg, "Optimisation of electrical system for offshore wind farms via genetic algorithm," *IET Renewable Power Generation*, vol. 3, no. 2, p. 205, Jun. 2009.

[22] G. Abeynayake, T. V. Acker, D. V. Hertem *et al.*, "Analytical model for availability assessment of large-scale offshore wind farms including their collector system," *IEEE Transactions on Sustainable Energy*, vol. 12, no. 4, pp. 1974-1983, Apr. 2021.

[23] R. Tan, P. Yang, P. He *et al.*, "Analysis on reliability and sensitivity of collection system of offshore wind farms considering electrical faults and switchgear configurations," *Power System Technology*, vol. 37, no. 8, pp. 2264-2270, Aug. 2013.

[24] X. Chen, B. Wang, and H. Deng *et al.*, "Analysis of the switchgear configuration for the ring collection grids of offshore wind farms," *Renewable Energy Resources*, vol. 37, no. 2, pp. 205-211, Feb. 2019.

[25] A. Sannino, H. Breder, and E. K. Nielsen, "Reliability of collection grids for large offshore wind parks," in *Proceedings of 2006 International Conference on Probabilistic Methods Applied to Power Systems*, Stockholm, Sweden, Jun. 2006, pp. 1-6.

[26] B. Wang, X. Wang, X. Wang, *et al.*, "An analytical approach to evaluate the reliability of offshore wind power plants considering environmental impact," *IEEE Transactions on Sustainable Energy*, vol. 9, pp. 249-260, Jan. 2018.

[27] X. Shen, S. Li, and H. Li, "Large-scale offshore wind farm electrical

collector system planning: a mixed-integer linear programming approach," in *Proceedings of 2021 IEEE 5th Conference on Energy Internet and Energy System Integration (EI2)*, Taiyuan, China, Oct. 2021, pp. 1248-1253.
[28] Z. Li, W. Wu, X. Tai *et al.*, "Optimization model-based reliability assessment for distribution networks considering detailed placement of circuit breakers and switches," *IEEE Transactions on Power Systems*, vol. 35, pp. 3991-4004, Sept. 2020.
[29] Z. Wang, D. Lin, T. Yu *et al.*, "Explicit reliability incorporated switches planning of smart distribution system with high flexibility," *International Journal of Electrical Power & Energy Systems*, vol. 145, p. 108629, Feb. 2023.
[30] X. Shen, Q. Wu, H. Zhang *et al.*, "Optimal planning for electrical collector system of offshore wind farm with double-sided ring topology," *IEEE Transactions on Sustainable Energy*, vol. 14, no. 3, pp. 1624-1633, Jul. 2023.
[31] M. Lee, C. Lu, and H. Huang, "Reliability and cost analyses of electricity collection systems of a marine current farm – a Taiwanese case study," *Renewable and Sustainable Energy Reviews*, vol. 13, pp. 2012-2021, Oct. 2009.
[32] J.-A. Pérez-Rúa, S. Lumbreras, A. Ramos *et al.*, "Reliability-based topology optimization for offshore wind farm collection system," *Wind Energy*, vol. 25, no. 1, pp. 52-70, Jun. 2022.
[33] J.-A. Pérez-Rúa and N. A. Cutululis, "Electrical cable optimization in offshore wind farms – a review," *IEEE Access*, vol. 7, pp. 85796-85811, Jul. 2019.
[34] Kis-orca. (2024, Jan.). Kis-orca homepage. [Online]. Available: https://kis-orca.org/
[35] Meteoblue. (2024, Jan.). Meteoblue homepage. [Online]. Available: https://content.meteoblue.com/en
[36] S. Turner, D. Romero, P. Zhang *et al.*, "A new mathematical programming approach to optimize wind farm layouts," *Renewable Energy*, vol. 63, pp. 674-680, Mar. 2014.
[37] X. Ding. (2023, Dec.). Test cases for a smart switch configuration and reliability assessment method for offshore wind farm electrical collector system. [Online]. Available: https://doi. org/10.6084/m9. figshare. 24953406.v1
[38] X. Gong, S. Kuenzel, and B. C. Pal, "Optimal wind farm cabling," *IEEE Transactions on Sustainable Energy*, vol. 9, no. 3, pp. 1126-1136, Nov. 2017.
[39] T. Zuo, Y. Zhang, K. Meng *et al.*, "Collector system topology design for offshore wind farm's repowering and expansion," *IEEE Transactions on Sustainable Energy*, vol. 12, no. 2, pp. 847-859, Sept. 2020.
[40] T. Zuo, Y. Zhang, K. Meng *et al.*, "A two-layer hybrid optimization approach for large-scale offshore wind farm collector system planning," *IEEE Transactions on Industrial Informatics*, vol. 17, no. 11, pp. 7433-7444, Feb. 2021.

Xiaochi Ding received the B.Eng. degree in electrical engineering from China Agricultural University, Beijing, China, in 2022. He is currently pursuing a Master's degree at Tsinghua-Berkeley Shenzhen Institute, Tsinghua Shenzhen International Graduate School, Tsinghua University, Shenzhen, China. His research interests include power system reliability, decision-making under uncertainty, and design and analysis of graph algorithms.

Xinwei Shen received the B.Eng. and Ph.D. degrees from the Department of Electrical Engineering, Tsinghua University, Beijing, China, in 2010 and 2016, respectively. He was a Visiting Scholar with the Illinois Institute of Technology, Chicago, USA, University of California, Berkeley, USA, and the University of Macau, Macau, China, in 2014, 2017, and 2021, respectively. He is currently an Assistant Professor with Tsinghua Shenzhen International Graduate School, Tsinghua University, Shenzhen, China. His research interests include energy internet, integrated energy system, power distribution system, and ocean renewables optimization.

Qiuwei Wu received the Ph.D. degree in power system engineering from Nanyang Technological University, Singapore, in 2009. Since January 2022, he has been a Tenured Associate Professor with Tsinghua-Berkeley Shenzhen Institute, Tsinghua Shenzhen International Graduate School, Tsinghua University, Shenzhen, China. From March 2008 to October 2009, he was a Senior R&D Engineer with Vestas Technology R&D Singapore Pte Ltd., Singapore. From November 2009 to February 2022, he was with the Department of Electrical Engineering, Technical University of Denmark, Lyngby, Denmark, as a Postdoc from November 2009 to October 2010, Assistant Professor from Nov ember 2010 to August 2013, and Associate Professor September 2013 to August 2021. His research interests include decentralized/distributed optimal operation and control of power and energy systems with high penetration of renewables, distributed wind power modelling and control, decentralized/distributed congestion management, voltage control and load restoration of active distribution networks, and decentralized/distributed optimal operation of integrated energy systems.

Liming Wang received the B.S., M.S., and Ph.D. degrees in high-voltage engineering from the Department of Electrical Engineering, Tsinghua University, Beijing, China, in 1987, 1990, and 1993, respectively. Since 1993, he has been with Tsinghua University. His major research interests include high-voltage insulation and electrical discharge, flashover mechanism on contaminated insulators, and application of pulsed electric fields.

Dechang Yang received the M.S. degree in electrical engineering from China Agricultural University, Beijing, China, in 2008, and the Ph.D. degree in power system from TU Dortmund, Dortmund, Germany, in 2012. He is currently an Associate Professor with the China Agricultural University. His research interests include active distribution network operation and control, integrated multienergy system planning, economic dispatching, and optimal management.